



OPEN

SUBJECT AREAS:

ELECTRONIC PROPERTIES  
AND MATERIALSELECTRONIC AND SPINTRONIC  
DEVICES

APPLIED PHYSICS

ELECTRONIC DEVICES

# An efficient methodology for measurement of the average electrical properties of single one-dimensional NiO nanorods

Ranjit A. Patil<sup>1</sup>, Rupesh S. Devan<sup>1</sup>, Jin-Han Lin<sup>2</sup>, Yung Liou<sup>2</sup> & Yuan-Ron Ma<sup>1</sup>Received  
28 June 2013Accepted  
11 October 2013Published  
29 October 2013Correspondence and  
requests for materials  
should be addressed to  
Y.-R.M. (ronma@mail.  
ndhu.edu.tw)<sup>1</sup>Department of Physics, National Dong Hwa University, Hualien 97401, Taiwan, <sup>2</sup>Institute of Physics, Academia Sinica, Taipei, 11529, Taiwan.

We utilized a metal tantalum (Ta) ball-probe to measure the electrical properties of vertical-aligned one-dimensional (1D) nickel-oxide (NiO) nanorods. The 1D NiO nanorods (on average, ~105 nm wide and ~700 nm long) are synthesized using the hot-filament metal-oxide vapor deposition (HFMOVD) technique, and they are cubic phased and have a wide bandgap of 3.68 eV. When the 1D NiO nanorods are arranged in a large-area array in ohmic-contact with the Ta ball-probe, they acted as many parallel resistors. By means of a rigorous calculation, we can easily acquire the average resistance  $R_{NR}$  and resistivity  $\rho_{NR}$  of a single NiO nanorod, which were approximately  $3.1 \times 10^{13} \Omega$  and  $4.9 \times 10^7 \Omega \cdot \text{cm}$ , respectively.

Recently researchers have become very engrossed in studies of transition metal oxide nanostructures<sup>1</sup>, because of their many unique characteristics. For example, nickel oxide nanostructures possess various outstanding properties, such as a wide bandgap (~3.88 eV)<sup>2</sup>, large specific capacitance (~390 F/g)<sup>3</sup> for supercapacitor electrodes, high-performance discharge capacity (~638 mA h/g)<sup>4</sup> for lithium ion batteries, high carrier density ( $\sim 7.35 \times 10^{18} \text{ cm}^{-3}$ )<sup>5</sup>, rapid switching time (<10 ns)<sup>6</sup> for resistance-based memory, stable endurance (up to  $1 \times 10^6$  cycles)<sup>7</sup> for resistive switching, high photon-to-current conversion efficiency (~45%) for sandwich dye-sensitized solar cells<sup>8</sup>, high catalytic activity ( $42.3 \text{ gm}^{-2}$ ) for carbon-monoxide oxidation<sup>9</sup>, very fast coloration and bleaching times (1.55 and 1.22 s)<sup>10</sup> for electrochromic devices, and so on. NiO nanostructures can be fabricated in a variety of forms including nanowalls<sup>2,4</sup>, nanoslices<sup>3</sup>, nanoplates<sup>3</sup>, nanoparticles<sup>5</sup>, nanofilaments<sup>6</sup>, nanowires<sup>7,11</sup>, nanocolumns<sup>3,9</sup>, nanotubes<sup>11,12</sup>, and nanorods<sup>11,13</sup>. However, one-dimensional (1D) nanostructures like nanowires and nanorods are more suitable than the other zero- and two-dimensional nanostructures for applications in electronic nanodevices. For example, the 1D forms can be used for electrical transmission lines, electrodes and electrical probes. All of this has made the exploration of the electrical properties of these 1D nanostructures very important. However, to the best of our knowledge, there have been only two studies reporting the electrical properties of single 1D NiO nanowires<sup>14,15</sup>. Clearly, more investigations of the electrical properties of 1D NiO nanostructures are necessary.

In this study a tantalum (Ta) ball-probe is utilized as an electrode to make direct contact with the vertical-aligned 1D NiO nanorods for measurement of the average electrical properties of single 1D NiO nanorods at room temperature. The current-voltage ( $I$ - $V$ ) results show the nanocontacts between the Ta-metal ball-probe and the 1D NiO nanorods to be ohmic contacts. Very large currents, up to several hundred milliamperes (mA), are able to pass through the ohmic nanocontacts, without damaging the 1D NiO nanorods. This is because the vertical-aligned 1D NiO nanorods acted as parallel resistors when in contact with the Ta ball probe. Using rigorous calculation, the average resistance  $R_{NR}$  and resistivity  $\rho_{NR}$  of a single NiO nanorod can be derived by averaging the number of parallel vertical-aligned 1D NiO nanorods. The average resistance  $R_{NR}$  and resistivity  $\rho_{NR}$  are  $\sim 3.1 \times 10^{13} \Omega$  and  $4.9 \times 10^7 \Omega \cdot \text{cm}$ , respectively. The large average resistance  $R_{NR}$  and large difference in the conductivity at small and relatively high voltages indicate the 1D NiO nanorods to be a good insulator and an excellent candidate for resistance switching devices. The ball-probe technique is a simple and effective method to explore the electrical properties of 1D nanostructures.

Vertical-aligned 1D NiO nanorod (or nanowire) arrays are difficult to synthesize by conventional chemical reaction<sup>2,3,7-9,11</sup> and thermal oxidation deposition techniques<sup>4,5,12,13</sup>. In this study, we are able to synthesize



large-area arrays of vertical-aligned 1D NiO nanorods using the hot-filament metal-oxide vapor deposition (HFMOVD) technique. This technique has become very important, because it can be used to synthesize a variety of metal-oxide<sup>10,16–26</sup> and metal<sup>27–30</sup> nanostructures with diverse morphological features and crystalline traits. The 1D NiO nanorods thus produced were then characterized by field-emission scanning electron microscopy (FESEM), energy dispersive spectroscopy (EDS), transmission electron microscopy (TEM), x-ray diffractometry (XRD) and ultraviolet-visible spectroscopy.

## Results

The FESEM images in the Fig. 1(a) show the top view of a large-area array of 1D NiO nanorods uniformly distributed on a *p*-type Si wafer. The array contains  $\sim 20$  nanorods per square micrometer. The high magnification FESEM image in Fig. 1(b) displays the flat and rectangular ends of the 1D NiO nanorods, which are clearly rectangular in shape. Fig. 1(c) displays a statistical histogram of the width distribution of the rectangular 1D nanorods. It is clear that a large number of the 1D nanorods fall in the 80–120 nm range. Most have a width of about 100–105 nm, with the average width being approximately  $\sim 105$  nm. The varying widths can be fitted to a log-normal distribution function (Eq. (1)),

$$f_N(w) = \frac{A}{w\sigma\sqrt{2\pi}} \exp\left[-\frac{\ln(w/\hat{w})^2}{2\sigma^2}\right] \quad (1)$$

where  $w$  is the width of the nanorod;  $\hat{w}$  ( $=105.4 \pm 0.6$  nm) is the mean (average) width of various nanorods;  $A$  ( $=480 \pm 7.5$ ) is the initial constant; and  $\sigma$  ( $=0.21 \pm 0.007$ ) is the standard deviation of the widths of the nanorods. The log-normal distribution of the nanorod widths is asymmetrical. The small standard deviation of the width distribution ( $\sigma \leq 0.25$ ) indicates that it is very well confined to a limited width range. The length distribution of the 1D NiO nanorods can be also statistically gathered and fitted by the log-normal distribution function (Fig. S1, Supporting Information). The statistical histogram in Fig. S1 displays the length distribution of the 1D NiO nanorods. The mean length of the nanorods and the standard deviation of the lengths are  $700 \pm 9$  nm and  $0.14 \pm 0.02$ , respectively. The standard deviation of the lengths is much smaller than that of the widths, implying most of the 1D NiO nanorods to be  $\sim 700$  nm long. Quantitative analysis of the chemical composition on the surface of the large-area array of 1D NiO nanorods was carried out by EDS. The EDS spectrum shown in Fig. 1(d) indicates that the 1D nanorods are composed of only the elements Ni and O. Note that the Si peak that occurs is due to the Si substrate. The crystalline

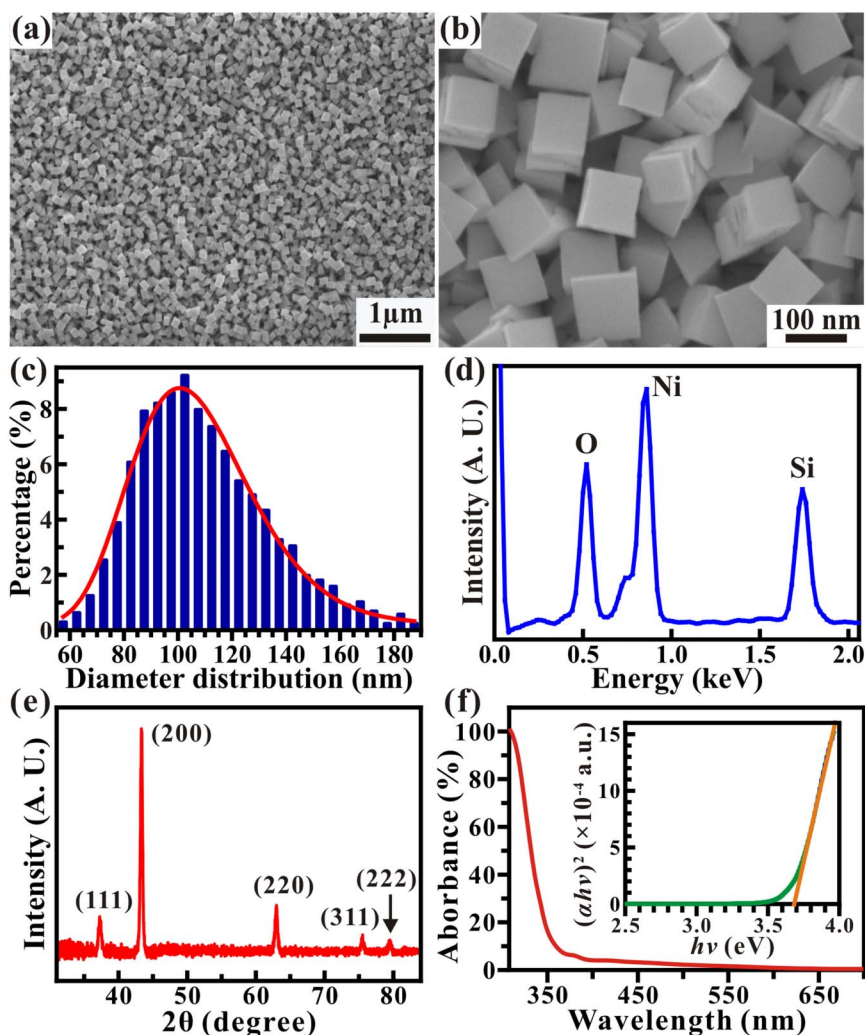


**Figure 1** | Characterization of 1D NiO nanorods. (a) FESEM image of the top view of the large-area array of vertical-aligned 1D NiO nanorods on a *p*-type Si wafer. (b) High magnification FESEM image displays the flat and sharp ends of the 1D NiO nanorods which shows rectangular in shape. (c) Statistical histogram of the width distribution of the nanorods, fitted by a log-normal distribution function. (d) EDS spectrum of the large-area array of 1D NiO nanorods. (e) Room-temperature XRD and (f) optical absorption spectra of the 1D NiO nanorod array deposited on ITO. The  $(\alpha h\nu)^2$  vs.  $h\nu$  curve is plotted in the inset to (f) and the absorption-edge line extrapolated at  $E_g = 3.68$  eV.



structure of the 1D NiO nanorods is revealed by the XRD patterns. Fig. 1(e) shows the XRD pattern of 1D nickel oxide (NiO) nanorods. The XRD spectrum indicates that the large-area array of 1D NiO nanorods consists of only face centered cubic (fcc) phase, assigned to the space group  $Fm\bar{3}m$  with lattice constants  $a=b=c=4.1680\text{ \AA}$  and  $\alpha = \beta = \gamma = 90^\circ$  (JCPDS 47-1049). The diffraction peaks at  $2\theta = 37.2^\circ, 43.4^\circ, 63.0^\circ, 75.4^\circ,$  and  $79.4^\circ$  correspond to the (111), (200), (220), (311), and (222) lattice planes, respectively, and agree with the XRD results obtained in previous studies<sup>9,11,13</sup>. The TEM images and SAED pattern of a single 1D NiO nanorod (Fig. S2, Supplemental Information) indicate that the 1D NiO nanorods preferentially grow along the [200] direction. The high-magnification TEM images in Fig. S2 show portions of atomic-resolution lattice planes, taken from the edge regions in the selected areas. Also, the SAED pattern taken from the selected areas, illustrates a set of four-fold symmetric diffraction spots indexed to the [001] zone axis. The reflections in the SAED pattern are consistent with the XRD results, also indicating the 1D NiO nanorods to be comprised of cubic crystals. In addition, the optical properties of the 1D NiO nanorods can be explored using optical absorption spectroscopy. Fig. 1(f) shows that the optical absorption spectrum of 1D NiO nanorods at room temperature on indium tin oxide (ITO). More details of the synthesis and characterization of the 1D NiO nanorod on ITO coated glass substrate is reported previously<sup>10</sup>. The high absorbance in the UV region implies that the 1D NiO nanorods possess a wide bandgap. The band gap  $E_g$  of the 1D NiO nanorods can be determined by using equation<sup>31</sup>,

$$(\alpha hv)^n = A(hv - E_g), \quad (2)$$

where  $hv$  is the incident photon energy,  $\alpha$  is the absorption coefficient,  $E_g$  is the band gap of the 1D NiO nanorods,  $A$  is a constant, and  $n$  is either 2 or  $1/2$  for direct or indirect band transitions, respectively. It has been verified in a previous study<sup>31</sup> that NiO nanostructures have a direct bandgap, so  $n = 2$  for the 1D NiO nanorods. The inset to Fig. 1(f) displays a linear graph of the  $(\alpha hv)^2$  versus  $hv$  curve, according to Eq. (2). The orange line is used to indicate the fit of the  $(\alpha hv)^2$  vs.  $hv$  curve at the absorption edge and is extrapolated to the  $x$  axis at  $hw \approx 3.68\text{ eV}$ . The extrapolation result

indicates that the 1D NiO nanorods possess a wide bandgap of 3.68 eV, which agrees with those obtained in previous studies<sup>13,31</sup>.

The two schematic diagrams in Fig. 2(a) show the two metal-semiconductor junctions to be designated as the Ta/ $p$ -Si (the left panel) and the Ta/NiO-NRs/ $p$ -Si (the right panel) junctions, respectively, for  $I$ - $V$  measurements with the Ta ball-probe. The Ta ball-probe is approached to come into electrical contact with the  $p$ -type Si surface or with the free ends of the vertical-aligned 1D NiO nanorods grown on the  $p$ -type Si wafer. The resultant  $I$ - $V$  characteristics of the two Ta/ $p$ -Si and Ta/NiO-NRs/ $p$ -Si junctions can be measured directly at room temperature. In fact, many methods, such as, field-effect transistors (FET)<sup>32</sup>, contact-mode atomic force microscopy (CM-AFM)<sup>33</sup>, and two/four probe contact techniques<sup>14,34,35</sup>, have been used to measure the  $I$ - $V$  characteristics of 1D nanorods (or nanowires). These typical methods allow only very small currents of a few microamperes ( $\mu\text{A}$ ) or nanoamperes (nA) due to the large contact resistance which strongly and considerably affects the experimental result. In contrast to these typical methods, the Ta ball-probe method can offer very large currents up to several hundred milliamperes (mA) and even one ampere. This is because the 1D NiO nanorods in the large-area array act as plentiful parallel resistors in connection with the Ta ball probe. Although each parallel resistor undergoes a small current, all parallel resistors together can bear very large currents. The left and right-hand panels in Fig. 2(b) show schematic diagrams of the electrical circuits corresponding to the Ta/ $p$ -Si and the Ta/NiO-NRs/ $p$ -Si junctions, respectively, shown in Fig. 2(a). The resistance ( $\equiv R_{\text{Ta/Si}}$ ) of the Ta/ $p$ -Si junction is equivalent to three resistors in series

$$R_{\text{Ta/Si}} = R_c + R_{\text{Si}} + R_e, \quad (3)$$

where  $R_c$  is the specific contact resistance between the Ta ball-probe and the  $p$ -type Si surface;  $R_{\text{Si}}$  is the resistance of the  $p$ -type Si surface; and  $R_e$  is the resistance of electrodes. Likewise, the resistance ( $\equiv R_{\text{Ta/NR/Si}}$ ) of the Ta/NiO-NRs/ $p$ -Si junction is equal to a combination of the specific nanocontact resistances ( $\equiv R_{\text{nc}}$ ) of the Ta ball-probe in contact with a single 1D NiO nanorod, the average resistance ( $\equiv R_{\text{NR}}$ ) of a single 1D NiO nanorod, and the two resistances  $R_{\text{Si}}$  and  $R_e$ , that is

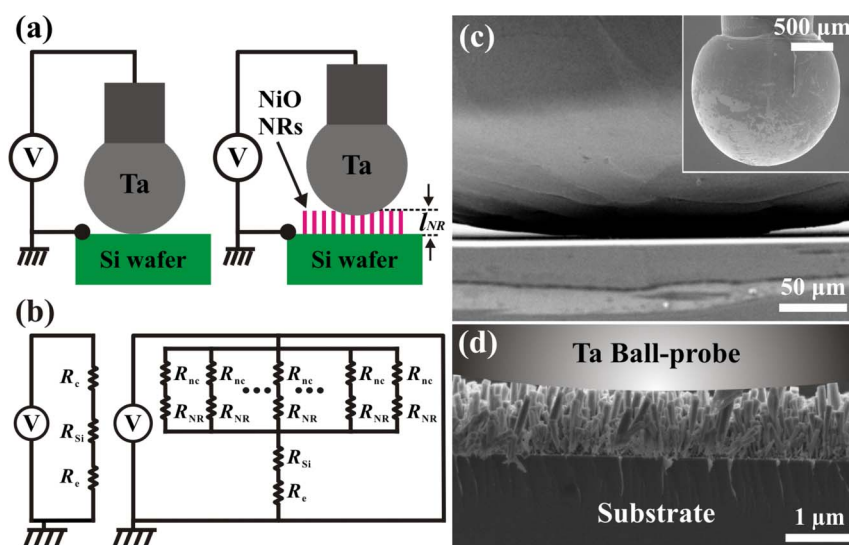


**Figure 2** |  $I$ - $V$  measurement setup. (a) Two schematic diagrams of the Ta/ $p$ -Si (left-hand panel) and the Ta/NiO-NRs/ $p$ -Si (right-hand panel) junctions for  $I$ - $V$  measurements with a Ta ball-probe. (b) Two schematic diagrams of the electrical circuits in the left and right panels corresponding to the Ta/ $p$ -Si and the Ta/NiO-NRs/ $p$ -Si junctions, respectively, in fig. 1(a). (c) FESEM images of a Ta ball-probe in contact with the 1D NiO nanorod array. The inset to (c) shows a whole Ta ball-probe in contact with the 1D NiO nanorod array. (d) High magnification FESEM image of the 1D NiO nanorod array in contact with a Ta ball-probe. The 1D NiO nanorods vertically aligned to the Ta ball-probe and substrate surface. The vertically aligned 1D NiO nanorods are on average  $\sim 700\text{ nm}$  ( $\equiv l_{\text{NR}}$ ) long.



$$R_{\text{Ta}/\text{NR}/\text{Si}} = (R_{\text{nc}} + R_{\text{NR}})/m + R_{\text{Si}} + R_{\text{c}}, \quad (4)$$

where  $m$  is the number of parallel 1D NiO nanorods connected with the Ta ball-probe. The FESEM images in Fig. 2(c) display a Ta ball-probe in contact with the 1D NiO nanorod array. The diameter of the contact area ( $\equiv A_c$ ) is estimated to be  $\sim 100 \mu\text{m}$ . Hence, the contact area  $A_c (= \pi r^2)$  is  $\sim 7854 \mu\text{m}^2$ . The inset to Fig. 2(c) shows a Ta ball-probe with a radius  $L$  ( $\approx 750 \mu\text{m}$ ). The high magnification FESEM image in Fig. 2(d) clearly shows the idea that how the Ta ball-probe was in contact with the large-area array of rectangular 1D NiO nanorods, and illustrating the rectangular 1D NiO nanorods vertically aligned to the Ta ball-probe on Si surface. It can be also seen that the vertically aligned 1D NiO nanorods are on average  $\sim 700 \text{ nm}$  ( $\equiv l_{\text{NR}}$ ) long.

## Discussion

The graph in Fig. 3(a) shows two room temperature  $I$ - $V$  curves for the metal-semiconductor Ta/ $p$ -Si and Ta/NiO-NRs/ $p$ -Si junctions. These two  $I$ - $V$  curves are symmetrical, non-rectifying, and linear in the small voltage range, implying that the Ta/ $p$ -Si and Ta/NiO-NRs/ $p$ -Si junctions have ohmic-contact characteristics. In Fig. 3(b), it can be seen that both  $I$ - $V$  curves are almost linear between  $-0.4$  to  $0.4 \text{ V}$ . As known, the work functions  $\varphi_{\text{Ta}}$ ,  $\varphi_{\text{NiO}}$ , and  $\varphi_{\text{Si}}$  of Ta, NiO, and Si are  $4.21^{36}$ ,  $4.3^4$ , and  $4.83^{37} \text{ eV}$ , respectively. Since  $\varphi_{\text{NiO}} > \varphi_{\text{Ta}}$  and  $\varphi_{\text{Si}} > \varphi_{\text{Ta}}$ , and NiO is a  $p$ -type semiconductor<sup>10</sup>, indicates the Ta/ $p$ -Si and Ta/NiO-NRs/ $p$ -Si junctions possess the ohmic-contact characteristics. Ohmic contacts constantly offer small resistance for conduction in both directions between a metal-semiconductor. Ideally, when a small voltage is applied, the current ( $I$ ) passing through the ohmic-contact junctions is a linear function of the small applied voltage. The ohmic resistance is determined to be the reciprocal of the  $dI/dV$  at  $0 \text{ V}$ <sup>38</sup>. The two zero-voltage ohmic resistances of  $R_{\text{Ta}/\text{Si}}$  and  $R_{\text{Ta}/\text{NR}/\text{Si}}$  are about  $8.0$  and  $2.0 \times 10^8 \Omega$ , respectively. In comparison with  $R_{\text{Ta}/\text{NR}/\text{Si}}$ ,  $R_{\text{Ta}/\text{Si}}$  is too small and can be ignored, so the difference in resistance between two ohmic junctions is  $2.0 \times 10^8 \Omega$ , as shown below

$$R_{\text{Ta}/\text{NR}/\text{Si}} - R_{\text{Ta}/\text{Si}} = (R_{\text{NR}}/m) + (R_{\text{nc}}/m) - R_{\text{c}} = 2.0 \times 10^8 \Omega. \quad (5)$$

The typical specific contact resistance  $R_{\text{c}}$  is small relative to those of the series of Si surfaces and electrodes. However, the specific nanocontact resistance  $R_{\text{nc}}$  is hundreds or thousands of times larger than the typical specific contact resistance  $R_{\text{c}}$ <sup>39</sup>, because the contact area ( $\equiv A_c$ ) of the typical metal-semiconductor junction is two or three orders of magnitude larger than the nanocontact area ( $\equiv A_{\text{nc}}$ ) of the metal-nanorod junction. The specific nanocontact resistance  $R_{\text{nc}}$  can be also determined by<sup>40</sup>

$$R_{\text{nc}} = \rho_{\text{c-NiO}}/A_{\text{nc}}, \quad (6)$$

where,  $\rho_{\text{c-NiO}}$  is the specific nanocontact resistivity and  $A_{\text{nc}}$  is the nanocontact area between the Ta ball-probe and the nanorods. Similarly, the specific contact resistance  $R_{\text{c}}$  can be determined by

$$R_{\text{c}} = \rho_{\text{c-Si}}/A_{\text{c}}, \quad (7)$$

where,  $\rho_{\text{c-Si}}$  is the specific contact resistivity and  $A_{\text{c}}$  is the contact area between the Ta ball-probe and the  $p$ -type Si wafer. From Eq. (5), (6) and (7), we determine an average resistance  $R_{\text{NR}}$  for one single 1D NiO nanorod,

$$\begin{aligned} R_{\text{NR}} &= m \times 2.0 \times 10^8 \Omega + m \times R_{\text{c}} - R_{\text{nc}} \\ &= m \times 2.0 \times 10^8 \Omega + m \times \rho_{\text{c-Si}}/A_{\text{c}} - \rho_{\text{c-NiO}}/A_{\text{nc}}. \end{aligned} \quad (8)$$

Obviously, the average single nanorod resistance  $R_{\text{NR}}$  is strongly dependent on the number  $m$  of 1D NiO nanorods connected to the Ta ball-probe. As shown in Fig. 2(c), the diameter of the contact area  $A_{\text{c}}$  is estimated to be  $\sim 100 \mu\text{m}$ , so the contact area  $A_{\text{c}}$  is

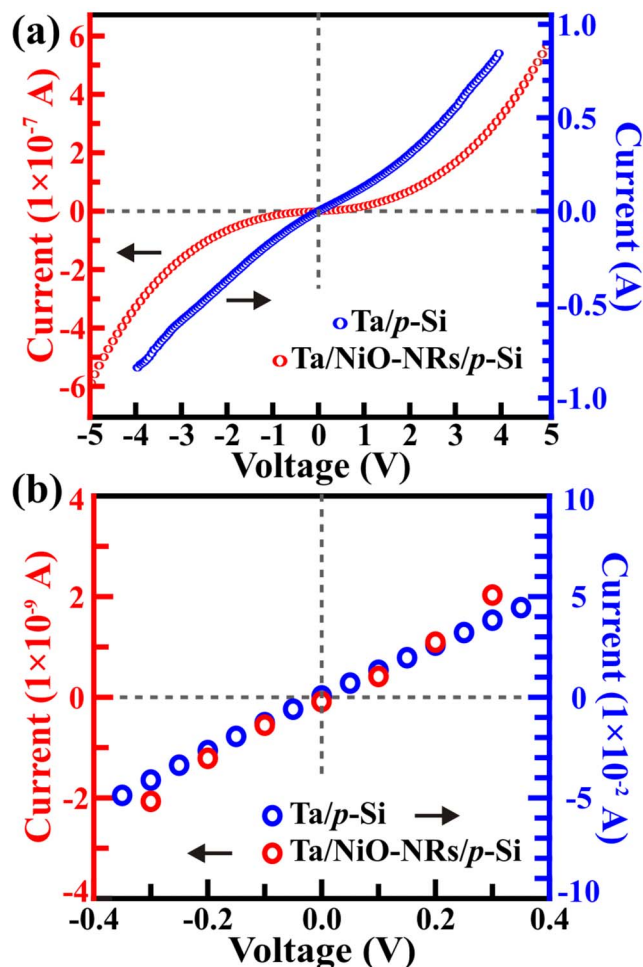


**Figure 3** |  $I$ - $V$  curves for the Ta/ $p$ -Si and the Ta/NiO-NRs/ $p$ -Si junctions. (a) Linear graph showing two room temperature  $I$ - $V$  curves for the metal-semiconductor Ta/ $p$ -Si and the Ta/NiO-NRs/ $p$ -Si junctions. (b) Linear graph displaying that both  $I$ - $V$  curves are almost linear between  $-0.4$  to  $0.4 \text{ V}$ .

$\sim 7854 \mu\text{m}^2$ . The array shown in Fig. 1(a) contains  $\sim 20$  nanorods per square micrometer, meaning that the contact area  $A_{\text{c}}$  contains  $157080 (= m)$  parallel 1D NiO nanorods connected with the Ta ball-probe. The average width  $\hat{w}$  of the 1D NiO nanorods is  $\sim 105 \text{ nm}$ , so the nanocontact area  $A_{\text{nc}} = \hat{w}^2 \approx 11025 \text{ nm}^2 \approx 1.1 \times 10^{-2} \mu\text{m}^2$ . In this study,  $A_{\text{nc}}$  is 6 orders of magnitude larger than  $A_{\text{c}}$ . Therefore, the average resistance  $R_{\text{NR}}$  of one single 1D NiO nanorod is

$$R_{\text{NR}} \approx 3.1 \times 10^{13} \Omega + 2.0 \times 10^9 \text{ cm}^{-2} \times \rho_{\text{c-Si}} - 9.1 \times 10^{10} \text{ cm}^{-2} \times \rho_{\text{c-NiO}}. \quad (9)$$

The specific contact resistivity for the metal-semiconductor junction is associated with a doping concentration<sup>40</sup>, and it is calculated by

$$\rho_{\text{c}} \propto \exp\left(\frac{4\pi\Phi_b\sqrt{\epsilon m^*}}{h\sqrt{N_a}}\right) \quad (10)$$

where,  $\Phi_b$  is the effective barrier height,  $m^*$  the effective mass,  $\epsilon$  the dielectric permittivity,  $h$  the Planck constant, and  $N_a$  the concentration of ionized acceptors in the semiconductor. As indicated in a previous study<sup>41</sup>, the typical specific contact resistivity of the ohmic contacts ranges from  $10^{-8}$  to  $10^{-6} \Omega\text{cm}^2$ , no matter how the chemical compositions differ across the metal-semiconductor junction, and how the doping concentrations vary in the semiconductor. Therefore, according to Eqs. (6) and (7), the values of  $\rho_{\text{c-Si}}$  and  $\rho_{\text{c-NiO}}$  are supposed to be in the ranges of  $10^{-8}$  to  $10^{-6}$  and  $10^{-2}$  to  $1 \Omega\text{cm}^2$ , respectively. When  $\rho_{\text{c-Si}}$  and  $\rho_{\text{c-NiO}}$  are substituted into Eq. (9), the second and third terms are too small and can be ignored. Thus the average resistance  $R_{\text{NR}}$  of one single 1D NiO nanorod is



$$R_{NR} \approx 3.1 \times 10^{13} \Omega. \quad (11)$$

Clearly,  $R_{NR}$  looks very large, meaning the single 1D NiO nanorod is an excellent insulator and a good candidate for use in resistance switching. According to the resistivity definition<sup>40</sup>, we can determine the average resistivity ( $\equiv \rho_{NR}$ ) of a single 1D NiO nanorod as follows:

$$\rho_{NR} = R_{NR} A_{nc} / l_{NR} = 4.9 \times 10^7 \Omega \cdot \text{cm} \quad (12)$$

where  $l_{NR}$  ( $\approx 700 \text{ nm} = 7 \times 10^{-5} \text{ cm}$ ) and  $A_{nc}$  ( $= \widehat{w}^2 \approx 11025 \text{ nm}^2 \approx 1.1 \times 10^{-10} \text{ cm}^2$ ) are the average length and the average nanocontact area of the single NiO nanorod. In comparison with previous studies of NiO thin films with various resistivities ranging between  $\sim 1 \times 10^{-1}$  and  $\sim 1 \times 10^6 \Omega \cdot \text{cm}$ <sup>42</sup>, the average resistivity  $\rho_{NR}$  of a single NiO nanorod is quite reasonable. Consequently, the design of the metal ball-probe method is a simple but effective method to acquire the average resistance  $R_{NR}$  and resistivity  $\rho_{NR}$  of a single 1D metal-oxide nanorod through the metal-semiconductor junctions.

In fact, the *IV* curves (Fig. S3, Supplemental Information) were measured by the Ta ball-probe for various 1D metal-oxide nanostructures more than few hundred times at varying experimental conditions. Fig. S3(a) shows six *IV* curves for six various 1D NiO nanorod samples, and Fig. S3(b) displays *IV* curves at varying temperatures, respectively. Obviously, all the obtained *IV* curves are well smooth and get very little fluctuations, indicating that the *IV* measurement system is pretty stable, accurate, and reliable. The six *IV* curves of Fig. S3(a) are very similar to that of Fig. 3(a), so all average resistances of the 1D NiO nanorods obtained at any experimental run are quite similar to each other. In addition, all the 1D NiO nanorods are very rigid solid, so they are hardly deformed. When the ball-probe comes to contact the 1D NiO ball-probe top-down, varying pressures may occur to push the Ta ball-probe against the 1D NiO nanorods at various *IV* measurements. We found no much difference in all the *IV* measurements, implying that the *IV* measurements are not changed at various pressures on the nanorods. Therefore, the influence of the pressure on the *IV* measurements is not so significant. However, temperature is an important factor for *IV* measurements. For example, Fig. S3(b) shows the *IV* curves obtained at temperatures of 90, 130, 170, 300 K, respectively. These *IV*-curve results indicate temperature really and strongly affect *IV* curves much more than pressure.

In conclusion, we synthesized a large-area array of vertical-aligned 1D NiO nanorods with the hot-filament metal oxide-vapor deposition technique. The cubic phase 1D NiO nanorods were on average  $\sim 105 \text{ nm}$  wide and  $\sim 700 \text{ nm}$  long, and possessed a bandgap of 3.68 eV. When a Ta ball-probe was used to make contact with the 1D NiO nanorods in the large area array, they acted as plentiful parallel resistors in connection with the Ta ball probe. The ball-probe is rigorous and effective method for acquiring the average resistance and specific resistivity of a single 1D NiO nanorod, which is  $\sim 3.1 \times 10^{13} \Omega$  and  $\sim 4.9 \times 10^7 \Omega \cdot \text{cm}$ , respectively. The large difference in conductivity between the low and high voltages indicates the single 1D NiO can be a potential candidate for use in resistance switching.

## Methods

Large-area arrays of rectangular 1D NiO nanorods were synthesized by the hot-filament metal-oxide vapor deposition (HFMOVD) technique. Clean nickel (Ni) wires (99.99% pure) with a diameter of 1 mm were passed through a pure graphite disc fixed to two supporting Cu electrodes mounted in a vacuum chamber. Once the pressure of the deposition chamber was pumped down to 2 torr, an argon (99.995%) flow was introduced into the vacuum chamber at 100 standard cubic centimeters per minute (sccm). The Ni wires were heated to  $\sim 1200^\circ \text{C}$  for 50 minutes to generate the nickel vapor. As the hot nickel vapor encountered the residual oxygen (or leaking air) it reacted to form the NiO vapor. The NiO vapor met the *p*-type Si wafer placed on the graphite disc holder ( $\sim 2 \text{ mm}$  above the Ni wire) and then condensed into 1D NiO nanorods. The surface morphology of the as-synthesized large-area 1D NiO nanorod array thus produced was characterized by a field-emission scanning electron microscope (FESEM, JEOL JSM-6500F) equipped with an energy dispersive X-ray spectrometer (EDS, Oxford instrument INCA, X-sight 7557). Structural analysis of

single NiO nanorods were carried out using a transmission electron microscope (TEM, JEOL JEM-2100) with a selected-area electron diffractometer (SAED) at an accelerating voltage of 200 kV. The structural analysis of the 1D NiO nanorods was carried out using an X-ray diffractometer (XRD, Regaku D/Max-2500) with Cu K $\alpha$  radiation ( $\lambda = 1.541 \text{ \AA}$ ). The optical absorption properties of the 1D NiO nanorods were examined by a UV-visible dual beam spectrophotometer (Hitachi, U3010). A tantalum (Ta) ball-probe of radius  $\sim 0.75 \text{ mm}$  ( $\equiv L$ ) was used as an electrode for the current-voltage (*I-V*) measurements. The room-temperature *I-V* measurements of the large-area 1D NiO nanorod arrays were performed in a vacuum chamber at a pressure of  $\sim 2 \times 10^{-7}$  torr using a Keithley 2410 electrometer.

- Devan, R. S., Patil, R. A., Lin, J.-H. & Ma, Y.-R. One-dimensional metal-oxide nanostructures: recent developments in synthesis, characterization, and applications. *Adv. Funct. Mater.* **22**, 3326–3370 (2012).
- Kumari, L., Li, W. Z., Vannoy, C. H., Leblanc, R. M. & Wang, D. Z. Vertically aligned and interconnected nickel oxide nanowalls fabricated by hydrothermal route. *Cryst. Res. Technol.* **44**, 495–499 (2009).
- Zhang, X. *et al.* Synthesis of porous NiO nanocrystals with controllable surface area and their application as supercapacitor electrodes. *Nano Res.* **3**, 643–652 (2010).
- Varghese, B. *et al.* Fabrication of NiO nanowall electrodes for high performance lithium ion battery. *Chem. Mater.* **20**, 3360–3367 (2008).
- Chen, H.-L. & Yang, Y.-S. Effect of crystallographic orientations on electrical properties of sputter-deposited nickel oxide thin films. *Thin Solid Films* **516**, 5590–5596 (2008).
- Lee, M.-J. *et al.* Electrical manipulation of nanofilaments in transition-metal oxides for resistance-based memory. *Nano Lett.* **9**, 1476–1481 (2009).
- Oka, K. *et al.* Resistive-switching memory effects of NiO nanowire/metal junctions. *J. Am. Chem. Soc.* **132**, 6634–6635 (2010).
- Morandeira, A. *et al.* Improved photon-to-current conversion efficiency with a nanoporous *p*-type NiO electrode by the use of a sensitizer-acceptor dyad. *J. Phys. Chem. C* **112**, 1721–1728 (2008).
- Zhu, J. *et al.* Facile route to oriented nickel hydroxide nanocolumns and porous nickel oxide. *J. Phys. Chem. C* **111**, 5622–5627 (2007).
- Patil, R. A. *et al.* Efficient electrochromic properties of high-density and large-area arrays of one-dimensional NiO nanorods. *Sol. Energy Mater. Sol. Cells* **112**, 91–96 (2013).
- Xiong, S., Yuan, C., Zhang, X. & Qian, Y. Mesoporous NiO with various hierarchical nanostructures by quasi-nanotubes/nanowires/nanorods self-assembly: controllable preparation and application in supercapacitors. *CrystEngComm.* **13**, 626–632 (2011).
- Ren, Y. *et al.* Formation of nickel oxide nanotubes with uniform wall thickness by low-temperature thermal oxidation through understanding the limiting effect of vacancy diffusion and the kirkendall phenomenon. *Adv. Funct. Mater.* **20**, 3336–3342 (2010).
- Zhang, Z., Zhao, Y. & Zhu, M. NiO films consisting of vertically aligned cone-shaped NiO rods. *Appl. Phys. Lett.* **88**, 033101 (2006).
- Tresback, J. S., Vasiliev, A. L., Pature, N. P., Park, S.-Y. & Berger, P. R. Characterization and electrical properties of individual Au–NiO–Au heterojunction nanowires. *IEEE Trans. Nanotechnol.* **6**, 676–681 (2007).
- Herderick, E. D., Reddy, K. M., Sample, R. N., Draskovic, T. I. & Pature, N. P. Bipolar resistive switching in individual Au–NiO–Au segmented nanowires. *Appl. Phys. Lett.* **95**, 203505 (2009).
- Ma, Y.-R., Lin, C.-M., Yeh, C.-L. & Huang, R.-T. Synthesis and characterization of one-dimensional WO<sub>2</sub> nanorods. *J. Vac. Sci. Technol. B* **23**, 2141–2145 (2005).
- Ma, Y.-R. *et al.* Magnetic properties of large-area one-dimensional WO<sub>2</sub> and MoO<sub>2</sub> nanorods. *J. Magn. Magn. Mater.* **304**, E13–E15 (2006).
- Kumari, L. *et al.* X-ray diffraction and Raman scattering studies on large-area array and nano-branched structure of 1D MoO<sub>2</sub> nanorods. *Nanotechnology* **18**, 115717 (2007).
- Kumari, L., Lin, J.-H. & Ma, Y.-R. Synthesis of bismuth oxide nanostructures by an oxidative metal vapor phase deposition technique. *Nanotechnology* **18**, 295605 (2007).
- Kumari, L., Lin, J.-H. & Ma, Y.-R. One-dimensional Bi<sub>2</sub>O<sub>3</sub> nanohooks: Synthesis, characterization and optical properties. *J. Phys.: Condens. Matter* **19**, 406204 (2007).
- Devan, R. S. *et al.* X-ray diffraction study of a large-scale and high-density array of one-dimensional crystalline tantalum pentoxide nanorods. *Cryst. Growth Des.* **8**, 4465–4468 (2008).
- Devan, R. S. *et al.* High room-temperature photoluminescence of one-dimensional Ta<sub>2</sub>O<sub>5</sub> nanorod arrays. *Nanotechnology* **20**, 445708 (2009).
- Devan, R. S., Ho, W.-D., Wu, S.-Y. & Ma, Y.-R. Low-temperature phase transformation and phonon confinement in one-dimensional Ta<sub>2</sub>O<sub>5</sub> nanorods. *J. Appl. Crystallogr.* **43**, 498–503 (2010).
- Devan, R. S. *et al.* Investigation of high-temperature phase transformation in one-dimensional Ta<sub>2</sub>O<sub>5</sub> nanorods. *J. Appl. Crystallogr.* **43**, 1062–1067 (2010).
- Devan, R. S. *et al.* Electrochromic properties of large-area and high-density arrays of transparent one-dimensional  $\beta$ -Ta<sub>2</sub>O<sub>5</sub> nanorods on indium-tin-oxide thin-films. *Appl. Phys. Lett.* **98**, 133117 (2011).
- Devan, R. S. *et al.* Enhancement of green-light photoluminescence of Ta<sub>2</sub>O<sub>5</sub> nanoblock stacks. *Phys. Chem. Chem. Phys.* **13**, 13441–13446 (2011).



27. Kumari, L. *et al.* Effects of deposition temperature and thickness on the structural properties of thermal evaporated bismuth thin films. *Appl. Surf. Sci.* **253**, 5931–5938 (2007).
28. Kumari, L., Lin, J.-H. & Ma, Y.-R. Laser oxidation and wide-band photoluminescence of thermal evaporated bismuth thin films. *J. Phys. D-Appl. Phys.* **41**, 025405 (2008).
29. Devan, R. S. *et al.* Two-dimensional single-crystalline pure Zn hexagonal nanoplates: Size-controllable synthesis and X-ray diffraction study. *Nanoscale* **3**, 4339–4345 (2011).
30. Lin, J.-H. *et al.* Room-temperature wide-range photoluminescence and semiconducting characteristics of two-dimensional pure metallic Zn nanoplates. *RSC Adv.* **2**, 2123–2127 (2012).
31. Wang, X. *et al.* Optical and electrochemical properties of nanosized NiO via thermal decomposition of nickel oxalate nanofibre. *Nanotechnology* **16**, 37–39 (2005).
32. Ma, R. M., Dai, L. & Qin, G. G. High-performance nano-schottky diodes and nano-MESFETs made on single CdS nanobelts. *Nano Lett.* **7**, 868–873 (2007).
33. Park, W. I., Yi, G. C., Kim, J.-W. & Park, S.-M. Schottky nanocontacts on ZnO nanorod arrays. *Appl. Phys. Lett.* **82**, 4358–4360 (2003).
34. Chaudhry, A., Ramamurthi, V., Fong, E. & Islam, M. S. Ultra-low contact resistance of epitaxially interfaced bridged silicon nanowires. *Nano Lett.* **7**, 1536–1541 (2007).
35. Mohny, S. E. *et al.* Measuring the specific contact resistance of contacts to semiconductor nanowires. *Solid-State Electron.* **49**, 227–232 (2005).
36. Hopkins, B. J. & Riviere, J. C. Work function values from contact potential difference measurements. *Br. J. Appl. Phys.* **15**, 941–946 (1964).
37. Allen, F. G. & Gobeli, G. W. Work function, photoelectric threshold, and surface states of atomically clean silicon. *Phys. Rev.* **127**, 150–158 (1962).
38. Ma, Y. J. *et al.* Hopping conduction in single ZnO nanowires. *Nanotechnology* **16**, 746–749 (2005).
39. Lin, Y.-F. & Jian, W.-B. The impact of nanocontact on nanowire based nanoelectronics. *Nano Lett.* **8**, 3146–3150 (2008).
40. Stern, E., Cheng, G., Young, M. P. & Reed, M. A. Specific contact resistivity of nanowire devices. *Appl. Phys. Lett.* **88**, 053106 (2006).
41. Blank, T. V. & Gol'dberg, Y. A. Mechanisms of current flow in metal–semiconductor ohmic contacts. *Semiconductors* **41**, 1263–1292 (2007).
42. Ishihara, T. *et al.* Electrode dependence and film resistivity effect in the electric-field-induced resistance-switching phenomena in epitaxial NiO film. *Mater. Sci. Eng. B* **148**, 40–42 (2008).

## Acknowledgements

The authors would like to thank the National Science Council of the Republic of China for their financial support of this research under Contract Nos. NSC-101-2112-M-259-003-MY2, NSC-102-2923-M-259-001-MY3, and NSC-101-2811-M-259-002.

## Author contributions

Y.-R.M. conceived and designed the study. R.A.P. performed the experiments. R.A.P. and R.S.D. analyzed the data and produced results. J.-H.L. fabricated the ball-probe IV measurement system. Y.-R.M. and R.A.P. wrote the manuscript in consultation with Y.L.

## Additional information

Supplementary information accompanies this paper at <http://www.nature.com/scientificreports>

**Competing financial interests:** The authors declare no competing financial interests.

**How to cite this article:** Patil, R.A., Devan, R.S., Lin, J.-H., Liou, Y. & Ma, Y.-R. An efficient methodology for measurement of the average electrical properties of single one-dimensional NiO nanorods. *Sci. Rep.* **3**, 3070; DOI:10.1038/srep03070 (2013).



This work is licensed under a Creative Commons Attribution-NonCommercial-ShareAlike 3.0 Unported license. To view a copy of this license, visit <http://creativecommons.org/licenses/by-nc-sa/3.0>